2024 IEEE International Conference on Robotics and Automation (ICRA 2024)
May 13-17, 2024. Yokohama, Japan

Dual-IMU State Estimation for Relative Localization of Two Mobile Agents

Wenqian Lai, Ruonan Guo, and Kejian J. Wu

Abstract— **In this paper, we address the problem of relative localization of two mobile agents. Specifically, we consider the Dual-IMU system, where each agent is equipped with one IMU, and employs relative pose observations between them. Previous works, however, typically assumed known ego motion and ignored biases of the IMUs. Instead, we study the most general case of unknown biases for both IMUs. Besides the derivation of dynamic model equations of the proposed system, we focus on the observability analysis, for the observability under general motion and the unobservable directions arising from various special motions. Through numerical simulations, we validate our key observability findings and examine their impact on the estimation accuracy and consistency. Finally, the system is implemented to achieve effective relative localization of an HMD with respect to a vehicle moving in the real world.**

I. Introduction

Relative localization between two mobile agents is a fundamental problem in the field of robotics and has various applications, such as multi-robot tasking [1], target tracking [2], formation flight of aircraft [3], and the use of head-mounted displays (HMD) in moving vehicles [4] for virtual/augmented reality. In such cases, rather than focusing solely on the absolute poses of each agent in the global coordinate system, it is of great interest to obtain the relative pose and motion information of one agent with respect to the coordinate system of the other agent.

One commonly used sensor for localization is the Inertial Measurement Unit (IMU) due to its small size and light weight. An IMU provides measurements of angular velocity and linear acceleration of the platform, and has been successfully employed for single-agent localization [5]. However, in the context of relative localization, the use of IMU has two limitations: Firstly, it only offers motion information with respect to an inertial frame, whereas the agent serving as the reference frame is often in motion, creating a non-inertial frame. This leads to discrepancies between the measurements from a single IMU and the desired relative motion information. To address this issue, two IMUs can be employed, with one equipped on each agent (Dual-IMU). The other limitation lies in the prolonged use of IMU, which often results in pose drift due to biases and noise. To achieve better localization, IMU data can be complemented with global observations (e.g. GPS [6]), or relative observations between the agents [7], as global information may be unavailable.

For the Dual-IMU system with relative observations, existing works have several limitations. Firstly, there is no prior work that fully addresses all four biases of the two IMUs. However, this is necessary because IMU biases are often unknown and time-varying, hence need to be estimated online. Moreover, the observability properties of this system, with unknown biases, remain uncertain. Observability [8], being a fundamental aspect of state estimation systems, determines whether certain state directions are solvable or not, affecting the system's estimation accuracy and consistency [9].

In this paper, we introduce a general Dual-IMU state estimation system, with relative position and orientation measurements, for achieving relative localization between two mobile agents. We present the dynamic model equations of the proposed system, which jointly estimates the relative pose, velocity, and all four IMU biases from both agents. Subsequently, we focus on the observability analysis, addressing both the observability under general motion of the two agents and the unobservable directions resulting from special motion constraints commonly found in practical moving platforms. In summary, the main contributions are:

- We introduce a Dual-IMU estimation system with the most general case of all biases unknown, and derive the continuous and discrete-time system model equations.
- We prove that the system is locally weakly observable under the condition of general motion.
- We analytically determine the unobservable directions of the system that arise when two agents undergo various special motions, and identify motion cases where relative pose estimates are either degraded or unaffected.
- We verify the impact of the unobservable directions on estimation results through numerical simulations. Furthermore, in a real-world example to localize an HMD with respect to a moving vehicle, the proposed system is implemented and achieves high estimation accuracy and processing speed.

II. Related Work

A prevalent approach to achieve localization of a single agent in the global frame utilizes the integration of IMU data with additional observations, such as GNSS in traditional navigation systems [10], [11], visual information from cameras [12], [13], [14], [15], or Lidar scans [16], [17]. As for multi-agent localization, the problem is often referred to as cooperative localization/SLAM. A distributed multi-robot localization algorithm that utilizes relative observations between robots has been proposed by [18]. [7], [19] exploited distance and bearing measurements between two agents to analytically compute their relative pose. [20] introduced cooperative mapping based on relative pose graphs. [21] reported a distributed cooperative mapping framework.

As for IMU-based multi-agent systems with relative observations, [22] conducted experiments to demonstrate that relative position observations between two IMUs can mitigate

Authors are with XREAL, Inc. Email: {wqlai,rnguo,kejian}@xreal.com

the global position divergence. However, this system emphasized global pose states. Some studies focused on directly estimating the relative pose states, e.g., [23] used line-of-sight measurements between two air vehicles, and [24] employed ICP algorithm to obtain relative translation and rotation as observations.

Meanwhile, extensive studies have delved into the observability properties of single-agent localization systems. [25], [26] proved the four unobservable directions of visual-inertial systems under general motion. [27], [28] investigated the additional unobservable directions of such systems under certain special motions. [29], [30] analyzed the underlying cause of system inconsistency stemming from unobservable directions, and introduced the first-estimates Jacobian Extended Kalman Filter to improve estimation consistency. Similarly, for observability analysis of the multi-agent localization problem, [31] showed that when considering only relative observations, the absolute pose becomes unobservable. [32] used the example of two robots to analyze the observability with global or relative observations.

A common limitation of the aforementioned works on multi-agent localization, however, is that they assumed known ego motion of the robots, or ignored biases from some of the IMUs. In contrast, in this work, we consider the most general case of unknown biases from both agents' IMUs, and jointly estimate them. More importantly, we analytically study the observability properties of such system, under both general and special motion scenarios.

III. Dual-IMU State Estimation

This section describes the dynamic and measurement models of our Dual-IMU state estimation system. This system comprises two IMUs, the reference and target IMU, which are rigidly attached to the moving reference and target agent, respectively (Fig. 1).

A. System State and Dynamic Model

The system state is a 22×1 vector, as:

$$\mathbf{x} = \begin{bmatrix} {}^{I_1}\mathbf{p}_{I_2}^T & {}^{I_1}\mathbf{v}_{I_2}^T & {}^{I_1}\mathbf{q}_{I_2}^T & \mathbf{b}_{g_1}^T & \mathbf{b}_{g_2}^T & \mathbf{b}_{a_1}^T & \mathbf{b}_{a_2}^T \end{bmatrix}^T \tag{1}$$

where ${}^{I_1}\mathbf{p}_{I_2}$, ${}^{I_1}\mathbf{v}_{I_2}$, ${}^{I_1}\mathbf{q}_{I_2}$ are the position, linear velocity, and unit quaternion of orientation of target IMU $\{I_2\}$ with respect to reference IMU $\{I_1\}$ (see Fig. 1), $\mathbf{b}_{g_1}$, $\mathbf{b}_{a_1}$ are the gyroscope and accelerometer biases of I_1, and $\mathbf{b}_{g_2}$, $\mathbf{b}_{a_2}$ are the biases of I_2, respectively.

The IMU measurement model of the angular velocity ${}^{I_n}\boldsymbol{\omega}_m$ and the linear acceleration ${}^{I_n}\mathbf{a}_m$, $n = 1, 2$, are:

$$ {}^{I_n}\boldsymbol{\omega}_m(t) = {}^{I_n}\boldsymbol{\omega}(t) + \mathbf{b}_{g_n}(t) + \mathbf{n}_{g_n}(t) \tag{2}$$

$$ {}^{I_n}\mathbf{a}_m(t) = {}^{I_n}\mathbf{a}(t) + \mathbf{b}_{a_n}(t) + \mathbf{n}_{a_n}(t) \tag{3}$$

where ${}^{I_n}\boldsymbol{\omega}(t)$ and ${}^{I_n}\mathbf{a}(t)$ are the true angular velocity and linear acceleration in IMU frame, ${}^{I_n}\mathbf{a}(t) = \mathbf{C}^T({}^G\mathbf{q}_{I_n}(t))({}^G\mathbf{a}_{I_n}(t) - {}^G\mathbf{g})$, with $\mathbf{C}({}^G\mathbf{q}_{I_n}(t))$ the rotation matrix of IMU frame $\{I_n\}$ at time t with respect to global frame $\{G\}$, ${}^G\mathbf{g}$ the known gravitational acceleration, and $\mathbf{n}_{g_n}(t)$ and $\mathbf{n}_{a_n}(t)$ are modeled as zero-mean, white Gaussian noise processes.

From (2)-(3), we derive continuous-time system model:

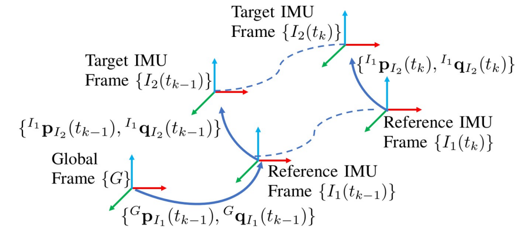

Fig. 1. The system comprises a static global coordinate frame $\{G\}$, and the moving reference and target IMU coordinate frames $\{I_1\}$ and $\{I_2\}$. ${}^{I_1}\mathbf{p}_{I_2}$ and ${}^{I_1}\mathbf{q}_{I_2}$ are the relative position and orientation of the target IMU with respect to the reference IMU.

$$ {}^{I_1}\dot{\mathbf{p}}_{I_2}(t) = {}^{I_1}\mathbf{v}_{I_2}(t) \tag{4}$$

$$\begin{aligned} {}^{I_1}\dot{\mathbf{v}}_{I_2}(t) = \mathbf{C}({}^{I_1}\mathbf{q}_{I_2}(t))\,{}^{I_2}\mathbf{a}(t) - {}^{I_1}\mathbf{a}(t) \\ - 2\,{}^{I_1}\boldsymbol{\omega}(t) \times {}^{I_1}\mathbf{v}_{I_2}(t) - {}^{I_1}\dot{\boldsymbol{\omega}}(t) \times {}^{I_1}\mathbf{p}_{I_2}(t) \\ - {}^{I_1}\boldsymbol{\omega}(t) \times ({}^{I_1}\boldsymbol{\omega}(t) \times {}^{I_1}\mathbf{p}_{I_2}(t)) \end{aligned} \tag{5}$$

$$ {}^{I_1}\dot{\mathbf{q}}_{I_2}(t) = \frac{1}{2}({}^{I_1}\mathbf{q}_{I_2}(t) \otimes {}^{I_2}\bar{\boldsymbol{\omega}}(t) - {}^{I_1}\bar{\boldsymbol{\omega}}(t) \otimes {}^{I_1}\mathbf{q}_{I_2}(t)) \tag{6}$$

$$ \dot{\mathbf{b}}_{a_n}(t) = \mathbf{n}_{wa_n}(t), \qquad \dot{\mathbf{b}}_{g_n}(t) = \mathbf{n}_{wg_n}(t) \tag{7}$$

where ${}^{I_n}\bar{\boldsymbol{\omega}} \triangleq \begin{bmatrix} 0 & {}^{I_n}\boldsymbol{\omega}^T \end{bmatrix}^T$, $n = 1, 2$. The IMU biases are modeled as random walks driven by zero-mean, white Gaussian noise $\mathbf{n}_{wg_n}$ and $\mathbf{n}_{wa_n}$. For derivation see Appendix A in our Supp. Mater. [33].

B. Continuous-Time Error-State Equation

The linearized continuous-time error-state equation is:

$$\dot{\tilde{\mathbf{x}}}(t) = \mathbf{F}(t)\tilde{\mathbf{x}}(t) + \mathbf{G}(t)\mathbf{n}(t) \tag{8}$$

where $\tilde{\mathbf{x}}$ is the 21×1 error state of (1). For the position, velocity, and bias states, the additive error model is used, i.e., $\tilde{\mathbf{x}} = \mathbf{x} - \hat{\mathbf{x}}$ is the error of the estimate $\hat{\mathbf{x}}$ of the state $\mathbf{x}$. As for the quaternion state $\mathbf{q}$, the 3×1 angle error $\delta\boldsymbol{\theta}$ is defined as $\delta\mathbf{q} = \hat{\mathbf{q}}^{-1} \otimes \mathbf{q} = \begin{bmatrix} 1 & \frac{1}{2}\delta\boldsymbol{\theta}^T \end{bmatrix}^T$ following [34]. The continuous-time error-state transition matrix, $\mathbf{F}$, is:

$$\mathbf{F} = \begin{bmatrix} \mathbf{0}_3 & \mathbf{I}_3 & \mathbf{0}_3 & \mathbf{0}_3 & \mathbf{0}_3 & \mathbf{0}_3 & \mathbf{0}_3 \\ -\mathbf{U} & -2[{}^{I_1}\hat{\boldsymbol{\omega}}_\times] & -\hat{\mathbf{C}}[{}^{I_2}\hat{\mathbf{a}}_\times] & -\mathbf{K} & \mathbf{0}_3 & \mathbf{I}_3 & -\hat{\mathbf{C}} \\ \mathbf{0}_3 & \mathbf{0}_3 & -[{}^{I_2}\hat{\boldsymbol{\omega}}_\times] & \hat{\mathbf{C}}^T & -\mathbf{I}_3 & \mathbf{0}_3 & \mathbf{0}_3 \\ \mathbf{0}_3 & \mathbf{0}_3 & \mathbf{0}_3 & \mathbf{0}_3 & \mathbf{0}_3 & \mathbf{0}_3 & \mathbf{0}_3 \\ \mathbf{0}_3 & \mathbf{0}_3 & \mathbf{0}_3 & \mathbf{0}_3 & \mathbf{0}_3 & \mathbf{0}_3 & \mathbf{0}_3 \\ \mathbf{0}_3 & \mathbf{0}_3 & \mathbf{0}_3 & \mathbf{0}_3 & \mathbf{0}_3 & \mathbf{0}_3 & \mathbf{0}_3 \\ \mathbf{0}_3 & \mathbf{0}_3 & \mathbf{0}_3 & \mathbf{0}_3 & \mathbf{0}_3 & \mathbf{0}_3 & \mathbf{0}_3 \end{bmatrix}$$

$$\text{with } \hat{\mathbf{C}} \triangleq \mathbf{C}({}^{I_1}\hat{\mathbf{q}}_{I_2}), \qquad \mathbf{U} \triangleq [{}^{I_1}\hat{\boldsymbol{\omega}}_\times]^2 + [{}^{I_1}\dot{\hat{\boldsymbol{\omega}}}_\times] \tag{9}$$

$$\mathbf{K} \triangleq [{}^{I_1}\hat{\boldsymbol{\omega}}_\times][{}^{I_1}\hat{\mathbf{p}}_{I_2\times}] + [({}^{I_1}\hat{\boldsymbol{\omega}} \times {}^{I_1}\hat{\mathbf{p}}_{I_2} + 2{}^{I_1}\hat{\mathbf{v}}_{I_2})_\times]$$

and $\mathbf{n}$ is the noise, and $\mathbf{G}$ is the noise Jacobian matrix. For derivation see Appendix B in our Supp. Mater. [33].

C. Discrete-Time Error-State Equation

Given that the IMU measurements are acquired at discrete time steps, with two IMUs synchronized at each time interval $\delta t = t_k - t_{k-1}$, it is necessary to find the discrete-time error-state transition matrix $\boldsymbol{\Phi}_{k,k-1}$. The structure of $\boldsymbol{\Phi}$ is:

$$\boldsymbol{\Phi} = \begin{bmatrix} \boldsymbol{\Phi}_{11} & \boldsymbol{\Phi}_{12} & \boldsymbol{\Phi}_{13} & \boldsymbol{\Phi}_{14} & \boldsymbol{\Phi}_{15} & \boldsymbol{\Phi}_{16} & \boldsymbol{\Phi}_{17} \\ \boldsymbol{\Phi}_{21} & \boldsymbol{\Phi}_{22} & \boldsymbol{\Phi}_{23} & \boldsymbol{\Phi}_{24} & \boldsymbol{\Phi}_{25} & \boldsymbol{\Phi}_{26} & \boldsymbol{\Phi}_{27} \\ \mathbf{0}_3 & \mathbf{0}_3 & \boldsymbol{\Phi}_{33} & \boldsymbol{\Phi}_{34} & \boldsymbol{\Phi}_{35} & \mathbf{0}_3 & \mathbf{0}_3 \\ \mathbf{0}_3 & \mathbf{0}_3 & \mathbf{0}_3 & \mathbf{I}_3 & \mathbf{0}_3 & \mathbf{0}_3 & \mathbf{0}_3 \\ \mathbf{0}_3 & \mathbf{0}_3 & \mathbf{0}_3 & \mathbf{0}_3 & \mathbf{I}_3 & \mathbf{0}_3 & \mathbf{0}_3 \\ \mathbf{0}_3 & \mathbf{0}_3 & \mathbf{0}_3 & \mathbf{0}_3 & \mathbf{0}_3 & \mathbf{I}_3 & \mathbf{0}_3 \\ \mathbf{0}_3 & \mathbf{0}_3 & \mathbf{0}_3 & \mathbf{0}_3 & \mathbf{0}_3 & \mathbf{0}_3 & \mathbf{I}_3 \end{bmatrix} \tag{10}$$

The derivation and expression of each term in $\boldsymbol{\Phi}$ are provided in Appendix C in our Supp. Mater. [33].

D. Relative Pose Measurement Model

We consider two types of measurements in this paper, relative position ($\mathbf{dp}$) and relative orientation ($\mathbf{dq}$) measurements. These two measurement models are:

$$\mathbf{dp} = {}^{I_1}\mathbf{p}_{I_2} + \boldsymbol{\eta}_p, \qquad \mathbf{dq} = \begin{bmatrix} 1 & \frac{1}{2}\boldsymbol{\eta}_q^T \end{bmatrix}^T \otimes {}^{I_1}\mathbf{q}_{I_2} \tag{11}$$

where $\boldsymbol{\eta}_p$ and $\boldsymbol{\eta}_q$ are zero-mean, white Gaussian noise.

We can apply the derived system dynamic and measurement models (4)-(11) to various estimation frameworks, such as the Extended Kalman Filter (EKF) [13] or optimization-based methods [35], to obtain the state estimates.

IV. Nonlinear Observability Analysis under General Motion

Next, we conduct an observability analysis of our Dual-IMU system. We employ the nonlinear observability analysis method in [8] to prove that our system, under the condition of general motion, is locally weakly observable. For expression simplicity, we transform the state (1) to:

$$\mathbf{x}' = \begin{bmatrix} {}^{I_1}\mathbf{p}_{I_2}^T & \mathbf{v}'^T & {}^{I_1}\mathbf{q}_{I_2}^T & \mathbf{b}_{g_1}^T & \mathbf{b}_{g_2}^T & \mathbf{b}_{a_1}^T & \mathbf{b}_{a_2}^T \end{bmatrix}^T \tag{12}$$

where $\mathbf{v}' = {}^{I_1}\mathbf{v}_{I_2} + {}^{I_1}\boldsymbol{\omega} \times {}^{I_1}\mathbf{p}_{I_2}$. Since $\mathbf{v}'$ is simply a change of variable as compared to ${}^{I_1}\mathbf{v}_{I_2}$, the subsequent observability results with (12) are equivalent to those with (1).

Now, we rewrite (4)-(7) in input-affine form as:

$$\begin{aligned}
\dot{\mathbf{x}}' &= \mathbf{f}_0 + \mathbf{f}_1\, {}^{I_1}\boldsymbol{\omega}_m + \mathbf{f}_2\, {}^{I_2}\boldsymbol{\omega}_m + \mathbf{f}_3\, {}^{I_1}\mathbf{a}_m + \mathbf{f}_4\, {}^{I_2}\mathbf{a}_m \\
\mathbf{f}_0 &= \begin{bmatrix} \mathbf{f}_p^T & \mathbf{f}_v^T & \mathbf{f}_q^T & \mathbf{0}_{1\times 12} \end{bmatrix}^T \\
\mathbf{f}_1 &= \begin{bmatrix} [{}^{I_1}\mathbf{p}_{I_2\times}]^T & [\mathbf{v}'_\times]^T & -\frac{1}{2}[{}^{I_1}\mathbf{q}_{I_2}]^T_{R(:,2:4)} & \mathbf{0}_{3\times 12} \end{bmatrix}^T \\
\mathbf{f}_2 &= \begin{bmatrix} \mathbf{0}_3 & \mathbf{0}_3 & \frac{1}{2}[{}^{I_1}\mathbf{q}_{I_2}]^T_{L(:,2:4)} & \mathbf{0}_{3\times 12} \end{bmatrix}^T \\
\mathbf{f}_3 &= \begin{bmatrix} \mathbf{0}_3 & -\mathbf{I}_3 & \mathbf{0}_{3\times 4} & \mathbf{0}_{3\times 12} \end{bmatrix}^T \\
\mathbf{f}_4 &= \begin{bmatrix} \mathbf{0}_3 & \mathbf{C}^T({}^{I_1}\mathbf{q}_{I_2}) & \mathbf{0}_{3\times 4} & \mathbf{0}_{3\times 12} \end{bmatrix}^T \\
\text{with } \mathbf{f}_p &= \mathbf{v}' + \mathbf{b}_{g_1} \times {}^{I_1}\mathbf{p}_{I_2} \\
\mathbf{f}_v &= -\mathbf{C}({}^{I_1}\mathbf{q}_{I_2})\mathbf{b}_{a_2} + \mathbf{b}_{a_1} + \mathbf{b}_{g_1} \times \mathbf{v}' \\
\mathbf{f}_q &= -\frac{1}{2}([{}^{I_1}\mathbf{q}_{I_2}]_L \bar{\mathbf{b}}_{g_2} - [{}^{I_1}\mathbf{q}_{I_2}]_R \bar{\mathbf{b}}_{g_1})
\end{aligned} \tag{13}$$

where $[\mathbf{q}]_L$ and $[\mathbf{q}]_R$ are the left and right quaternion-multiplication matrices of $\mathbf{q}$, $\bar{\mathbf{b}}_{g_n} \triangleq \begin{bmatrix} 0 & \mathbf{b}_{g_n}^T \end{bmatrix}^T$, $n = 1, 2$. For derivation see Appendix D-1 in our Supp. Mater. [33].

As for system observations, the unit norm of ${}^{I_1}\mathbf{q}_{I_2}$ is treated as a measurement denoted by $\mathbf{h}_0$. Additionally, we include the $\mathbf{dp}$ measurement in our analysis, denoted by $\mathbf{h}_1$:

$$\mathbf{h}_0 = 1 = ||\, {}^{I_1}\mathbf{q}_{I_2}||_2^2, \qquad \mathbf{h}_1 = \mathbf{dp} = {}^{I_1}\mathbf{p}_{I_2} \tag{14}$$

Based on the approach outlined in [8], we found an observability submatrix formed by the following subset of Lie derivatives:

$$\begin{aligned}
&\boldsymbol{L}^0\boldsymbol{h_0},\ \boldsymbol{L}^0\boldsymbol{h_1},\ \boldsymbol{L}^1_{f_0}\boldsymbol{h_0},\ \boldsymbol{L}^1_{f_0}\boldsymbol{h_1},\ \boldsymbol{L}^2_{f_0f_0}\boldsymbol{h_1},\ \boldsymbol{L}^2_{f_0f_{41}}\boldsymbol{h_1}, \\
&\boldsymbol{L}^2_{f_0f_{42}}\boldsymbol{h_1},\ \boldsymbol{L}^2_{f_0f_{43}}\boldsymbol{h_1},\ \boldsymbol{L}^3_{f_0f_0f_{31}}\boldsymbol{h_1},\ \boldsymbol{L}^3_{f_0f_0f_{32}}\boldsymbol{h_1},\ \boldsymbol{L}^3_{f_0f_{41}f_0}\boldsymbol{h_1}, \\
&\boldsymbol{L}^3_{f_0f_{42}f_0}\boldsymbol{h_1},\ \boldsymbol{L}^3_{f_0f_{43}f_0}\boldsymbol{h_1},\ \boldsymbol{L}^3_{f_0f_0f_{21}}\boldsymbol{h_1},\ \boldsymbol{L}^3_{f_0f_0f_{22}}\boldsymbol{h_1}
\end{aligned} \tag{15}$$

This matrix has full column rank, which indicates that the system (13)-(14) is locally weakly observable. For detailed proof see Appendix D-2 in our Supp. Mater. [33].

In summary, we have shown that the Dual-IMU state estimation system with only $\mathbf{dp}$ measurement is observable. Hence, the case with both $\mathbf{dp}$ and $\mathbf{dq}$ measurements is also observable, trivially. This means that, if the two agents keep moving generally, the estimation results can be reliable.

V. Unobservable Directions under Special Motions

In the preceding section, we have established that under general motion conditions, as long as $\mathbf{dp}$ measurement is present, all states are observable. Here, general motion refers to the case when both agents move freely, rotationally and translationally, in the 3D space. In practice, however, agents cannot persistently sustain rich 3D motions. For example, in the case of ground-moving robots, they mostly undergo special motion profiles, such as stationary, linear, or planar motions. Also, in the case of a person wearing an HMD and sitting inside a moving vehicle, the HMD may often be stationary or purely rotating with respect to the vehicle. In this section, we present the unobservable directions arising from different types of special motions, and explain their physical meanings, for the case when both $\mathbf{dp}$ and $\mathbf{dq}$ measurements are used, as well as for the case when only $\mathbf{dp}$ measurement is used. Following the methodology in [36] [26], unobservable directions can be found as the null space of the observability matrix of the linearized system.

A. Unobservable Directions with Both $\mathbf{dp}$ and $\mathbf{dq}$

For all types of special motions we consider here, the unobservable directions of the system with both $\mathbf{dp}$ and $\mathbf{dq}$ measurements are summarized in Table (I). For proof see Appendix E-1 in our Supp. Mater. [33]. We can query Table (I) to obtain the corresponding unobservable state directions, according to the motion constraints of the two IMUs. The union of all unobservable directions in Table (I) is:

$$\begin{aligned}
&[\mathbf{b}_{a+} \mid \mathbf{b}_{g+}]_{[21\times 3,\ 21\times 3]} \\
&= \begin{bmatrix}
\mathbf{0}_3 & \mathbf{0}_3 \\
\mathbf{0}_3 & \mathbf{0}_3 \\
\mathbf{0}_3 & \mathbf{0}_3 \\
\mathbf{0}_3 & \mathbf{I}_3 \\
\mathbf{0}_3 & \mathbf{C}^T({}^{I_1}\mathbf{q}_{I_2}(t_0)) \\
\mathbf{I}_3 & \mathbf{0}_3 \\
\mathbf{C}^T({}^{I_1}\mathbf{q}_{I_2}(t_0)) & \mathbf{0}_3
\end{bmatrix}
\end{aligned} \tag{16}$$

And the physical meaning of each direction is:

- $\mathbf{b}_{a+}$ is 3 dof of the composite accelerometer bias.
- $\mathbf{b}^{\boldsymbol{\omega}}_{a+} = \mathbf{b}_{a+} \cdot {}^{I_1}\boldsymbol{\omega}_{I_2}$ is 1 dof of the composite accelerometer bias along ${}^{I_1}\boldsymbol{\omega}_{I_2}$ direction.
- $\mathbf{b}_{g+}$ is 3 dof of the composite gyroscope bias.
- $\mathbf{b}^{\boldsymbol{\omega}}_{g+} = \mathbf{b}_{g+} \cdot {}^{I_1}\boldsymbol{\omega}_{I_2}$ is 1 dof of the composite gyroscope bias along ${}^{I_1}\boldsymbol{\omega}_{I_2}$ direction.
- $\mathbf{b}^{\boldsymbol{\alpha}}_{g+} = \mathbf{b}_{g+} \cdot \boldsymbol{\alpha}$ is 1 dof of the composite gyroscope bias along $\boldsymbol{\alpha}$ direction, where $\boldsymbol{\alpha}$ is defined in Table (I).

B. Unobservable Directions with Only $\mathbf{dp}$

Under the same types of special motions, the unobservable directions in the case with both $\mathbf{dp}$ and $\mathbf{dq}$ measurements, shown in Table (I), will also exist in the case with only $\mathbf{dp}$ measurement. Furthermore, the absence of $\mathbf{dq}$ measurement will lead to some *additional* unobservable directions. These additional unobservable directions are summarized in Table (II). For proof see Appendix E-2 in our Supp. Mater. [33]. Therefore, we can obtain the *total* unobservable state directions for the $\mathbf{dp}$ only case, by querying Table (I) and Table (II) and adding them together. The union of all additional unobservable directions in Table (II) is:

TABLE I

UNOBSERVABLE DIRECTIONS WITH BOTH $\mathbf{dp}$ AND $\mathbf{dq}$ MEASUREMENTS

Motion Constraints of Target IMU w.r.t. Reference IMU‡				Motion Constraints of Reference IMU†						
				${}^{I_1}\boldsymbol{\omega}=\mathbf{0}$			${}^{I_1}\boldsymbol{\omega} \parallel \boldsymbol{\alpha}$		${}^{I_1}\boldsymbol{\omega}$ dir. const. ${}^{I_1}\boldsymbol{\omega} \nparallel \boldsymbol{\alpha}$	${}^{I_1}\boldsymbol{\omega}$ unconstrained
				${}^{I_1}\mathbf{a}=\boldsymbol{\alpha}$	${}^{I_1}\mathbf{v} \parallel \boldsymbol{\alpha}$	${}^{I_1}\mathbf{v}$ dir. const. ${}^{I_1}\mathbf{v} \nparallel \boldsymbol{\alpha}$	${}^{I_1}\mathbf{a}=\boldsymbol{\alpha}$	${}^{I_1}\mathbf{v} \perp {}^{I_1}\boldsymbol{\omega}$	${}^{I_1}\mathbf{v} \perp {}^{I_1}\boldsymbol{\omega}$	${}^{I_1}\mathbf{v}$ unconstrained
${}^{I_1}\mathbf{p}_{I_2}$	${}^{I_1}\mathbf{v}_{I_2}$	${}^{I_1}\boldsymbol{\omega}_{I_2}$		I	II	III	IV	V	VI	VII
$\mathbf{p}=\mathbf{0}$	$\mathbf{v}=\mathbf{0}$	$\boldsymbol{\omega}=\mathbf{0}$	A	$\mathbf{b}_{a+}$,$\mathbf{b}_{g+}$			$\mathbf{b}_{a+}$,$\mathbf{b}_{g+}$		$\mathbf{b}_{a+}$,$\mathbf{b}_{g+}$	$\mathbf{b}_{a+}$,$\mathbf{b}_{g+}$
		$\boldsymbol{\omega}_x=\mathbf{0}\ \boldsymbol{\omega}_y=\mathbf{0}$	B	$\mathbf{b}^{\boldsymbol{\omega}}_{a+}$,$\mathbf{b}^{\boldsymbol{\omega}}_{g+}$			$\mathbf{b}^{\boldsymbol{\omega}}_{a+}$,$\mathbf{b}^{\boldsymbol{\omega}}_{g+}$		$\mathbf{b}^{\boldsymbol{\omega}}_{a+}$,$\mathbf{b}^{\boldsymbol{\omega}}_{g+}$	$\mathbf{b}^{\boldsymbol{\omega}}_{a+}$,$\mathbf{b}^{\boldsymbol{\omega}}_{g+}$
		Unconstrained	C	0			0		0	0
$\mathbf{p}_x=\mathbf{0}$ $\mathbf{p}_y=\mathbf{0}$ $\mathbf{p}_z\neq\mathbf{0}$	$\mathbf{v}=\mathbf{0}$	$\boldsymbol{\omega}=\mathbf{0}$	D	$\mathbf{b}_{a+}$,$\mathbf{b}_{g+}$			$\mathbf{b}_{a+}$,$\mathbf{b}^{\boldsymbol{\alpha}}_{g+}$		$\mathbf{b}_{a+}$	$\mathbf{b}_{a+}$
		$\boldsymbol{\omega}_x=\mathbf{0}\ \boldsymbol{\omega}_y=\mathbf{0}$	E	$\mathbf{b}^{\boldsymbol{\omega}}_{a+}$,$\mathbf{b}^{\boldsymbol{\omega}}_{g+}$			$\mathbf{b}^{\boldsymbol{\omega}}_{a+}$,$\mathbf{b}^{\boldsymbol{\omega}}_{g+}$		$\mathbf{b}^{\boldsymbol{\omega}}_{a+}$	$\mathbf{b}^{\boldsymbol{\omega}}_{a+}$
		Unconstrained	F	0			0		0	0
	$\mathbf{v}_x=\mathbf{0}$ $\mathbf{v}_y=\mathbf{0}$	$\boldsymbol{\omega}=\mathbf{0}$	G	$\mathbf{b}_{a+}$,$\mathbf{b}^{\boldsymbol{\alpha}}_{g+}$			$\mathbf{b}_{a+}$,$\mathbf{b}^{\boldsymbol{\alpha}}_{g+}$		$\mathbf{b}_{a+}$	$\mathbf{b}_{a+}$
		$\boldsymbol{\omega}_x=\mathbf{0}\ \boldsymbol{\omega}_y=\mathbf{0}$	H	$\mathbf{b}^{\boldsymbol{\omega}}_{a+}$,$\mathbf{b}^{\boldsymbol{\omega}}_{g+}$			$\mathbf{b}^{\boldsymbol{\omega}}_{a+}$,$\mathbf{b}^{\boldsymbol{\omega}}_{g+}$		$\mathbf{b}^{\boldsymbol{\omega}}_{a+}$	$\mathbf{b}^{\boldsymbol{\omega}}_{a+}$
		Unconstrained	J	0			0		0	0
$\mathbf{p}_x\neq\mathbf{0}$ $\mathbf{p}_y\neq\mathbf{0}$ $\mathbf{p}_z\neq\mathbf{0}$	$\mathbf{v}=\mathbf{0}$	$\boldsymbol{\omega}=\mathbf{0}$	K	$\mathbf{b}_{a+}$,$\mathbf{b}_{g+}$			$\mathbf{b}_{a+}$		$\mathbf{b}_{a+}$	$\mathbf{b}_{a+}$
		$\boldsymbol{\omega}_x=\mathbf{0}\ \boldsymbol{\omega}_y=\mathbf{0}$	L	$\mathbf{b}^{\boldsymbol{\omega}}_{a+}$,$\mathbf{b}^{\boldsymbol{\omega}}_{g+}$			$\mathbf{b}^{\boldsymbol{\omega}}_{a+}$		$\mathbf{b}^{\boldsymbol{\omega}}_{a+}$	$\mathbf{b}^{\boldsymbol{\omega}}_{a+}$
		Unconstrained	M	0			0		0	0
	$\mathbf{v}_x=\mathbf{0}$ $\mathbf{v}_y=\mathbf{0}$	$\boldsymbol{\omega}=\mathbf{0}$	N	$\mathbf{b}_{a+}$,$\mathbf{b}^{\boldsymbol{\alpha}}_{g+}$			$\mathbf{b}_{a+}$		$\mathbf{b}_{a+}$	$\mathbf{b}_{a+}$
		$\boldsymbol{\omega}_x=\mathbf{0}\ \boldsymbol{\omega}_y=\mathbf{0}$	O	$\mathbf{b}^{\boldsymbol{\omega}}_{a+}$,$\mathbf{b}^{\boldsymbol{\omega}}_{g+}$			$\mathbf{b}^{\boldsymbol{\omega}}_{a+}$		$\mathbf{b}^{\boldsymbol{\omega}}_{a+}$	$\mathbf{b}^{\boldsymbol{\omega}}_{a+}$
		Unconstrained	P	0			0		0	0
	Uncon-strained	$\boldsymbol{\omega}=\mathbf{0}$	Q	$\mathbf{b}_{a+}$			$\mathbf{b}_{a+}$		$\mathbf{b}_{a+}$	$\mathbf{b}_{a+}$
		$\boldsymbol{\omega}_x=\mathbf{0}\ \boldsymbol{\omega}_y=\mathbf{0}$	R	$\mathbf{b}^{\boldsymbol{\omega}}_{a+}$			$\mathbf{b}^{\boldsymbol{\omega}}_{a+}$		$\mathbf{b}^{\boldsymbol{\omega}}_{a+}$	$\mathbf{b}^{\boldsymbol{\omega}}_{a+}$
		Unconstrained	S	0			0		0	0

For the motions we consider here, they are classified according to motion constraints of reference IMU (Cols I-VII) and motion constraints of target IMU with respect to reference IMU (Rows A-S). Here, Cell VII-S represents general motion, while all other cells correspond to various special motions. $\mathbf{b}_{a+}$, $\mathbf{b}_{g+}$, $\mathbf{b}^{\boldsymbol{\omega}}_{a+}$, $\mathbf{b}^{\boldsymbol{\omega}}_{g+}$, and $\mathbf{b}^{\boldsymbol{\alpha}}_{g+}$ denote the corresponding unobservable directions. In this table, for case Col-I, $\boldsymbol{\alpha}$ is the constant local acceleration of reference IMU, while for the rest cases Cols II-VII, $\boldsymbol{\alpha}$ equals the constant negative local gravity in the reference IMU at initial moment ($-{}^{I_1}\mathbf{g}(t_0)$).

TABLE II

ADDITIONAL UNOBSERVABLE DIRECTIONS WITH ONLY $\mathbf{dp}$ MEASUREMENT

Motion Constraints of Target IMU w.r.t. Reference IMU‡				Motion Constraints of Reference IMU†						
				${}^{I_1}\boldsymbol{\omega}=\mathbf{0}$			${}^{I_1}\boldsymbol{\omega} \parallel \boldsymbol{\alpha}$		${}^{I_1}\boldsymbol{\omega}$ dir. const. ${}^{I_1}\boldsymbol{\omega} \nparallel \boldsymbol{\alpha}$	${}^{I_1}\boldsymbol{\omega}$ unconstrained
				${}^{I_1}\mathbf{a}=\boldsymbol{\alpha}$	${}^{I_1}\mathbf{v} \parallel \boldsymbol{\alpha}$	${}^{I_1}\mathbf{v}$ dir. const. ${}^{I_1}\mathbf{v} \nparallel \boldsymbol{\alpha}$	${}^{I_1}\mathbf{a}=\boldsymbol{\alpha}$	${}^{I_1}\mathbf{v} \perp {}^{I_1}\boldsymbol{\omega}$	${}^{I_1}\mathbf{v} \perp {}^{I_1}\boldsymbol{\omega}$	${}^{I_1}\mathbf{v}$ unconstrained
${}^{I_1}\mathbf{p}_{I_2}$	${}^{I_1}\mathbf{v}_{I_2}$	${}^{I_1}\boldsymbol{\omega}_{I_2}$		I	II	III	IV	V	VI	VII
$\mathbf{p}=\mathbf{0}$	$\mathbf{v}=\mathbf{0}$	$\boldsymbol{\omega}=\mathbf{0}$	A	$\boldsymbol{\theta}$, $\mathbf{b}^{\boldsymbol{\alpha}}_{g_1}$	$\boldsymbol{\theta}^{\boldsymbol{\alpha}}$,$\mathbf{b}^{\boldsymbol{\alpha}}_{g_1}$	$\boldsymbol{\theta}^{\boldsymbol{\beta}_1}$	$\boldsymbol{\theta}^{\boldsymbol{\alpha}}$,$\mathbf{b}^{\boldsymbol{\alpha}}_{g_1}$	0	0	0
		$\boldsymbol{\omega}_x=\mathbf{0}\ \boldsymbol{\omega}_y=\mathbf{0}$	B	$\boldsymbol{\theta}$, $\mathbf{b}^{\boldsymbol{\alpha}}_{g_1}$	$\boldsymbol{\theta}^{\boldsymbol{\alpha}}$,$\mathbf{b}^{\boldsymbol{\alpha}}_{g_1}$	$\boldsymbol{\theta}^{\boldsymbol{\beta}_1}$	$\boldsymbol{\theta}^{\boldsymbol{\alpha}}$,$\mathbf{b}^{\boldsymbol{\alpha}}_{g_1}$	0	0	0
		Unconstrained	C	$\boldsymbol{\theta}$, $\mathbf{b}^{\boldsymbol{\alpha}}_{g_1}$	$\boldsymbol{\theta}^{\boldsymbol{\alpha}}$,$\mathbf{b}^{\boldsymbol{\alpha}}_{g_1}$	$\boldsymbol{\theta}^{\boldsymbol{\beta}_1}$	$\boldsymbol{\theta}^{\boldsymbol{\alpha}}$,$\mathbf{b}^{\boldsymbol{\alpha}}_{g_1}$	0	0	0
$\mathbf{p}_x=\mathbf{0}$ $\mathbf{p}_y=\mathbf{0}$ $\mathbf{p}_z\neq\mathbf{0}$	$\mathbf{v}=\mathbf{0}$	$\boldsymbol{\omega}=\mathbf{0}$	D	$\boldsymbol{\theta}$, $\mathbf{b}^{\boldsymbol{\alpha}}_{g_1}$	$\boldsymbol{\theta}^{\boldsymbol{\alpha}}$,$\mathbf{b}^{\boldsymbol{\alpha}}_{g_1}$	$\boldsymbol{\theta}^{\boldsymbol{\beta}_1}$	$\boldsymbol{\theta}^{\boldsymbol{\alpha}}$,$\mathbf{b}^{\boldsymbol{\alpha}}_{g_1}$	0	0	0
		$\boldsymbol{\omega}_x=\mathbf{0}\ \boldsymbol{\omega}_y=\mathbf{0}$	E	$\boldsymbol{\theta}$, $\mathbf{b}^{\boldsymbol{\alpha}}_{g_1}$	$\boldsymbol{\theta}^{\boldsymbol{\alpha}}$,$\mathbf{b}^{\boldsymbol{\alpha}}_{g_1}$	$\boldsymbol{\theta}^{\boldsymbol{\beta}_1}$	$\boldsymbol{\theta}^{\boldsymbol{\alpha}}$,$\mathbf{b}^{\boldsymbol{\alpha}}_{g_1}$	0	0	0
		Unconstrained	F	$\boldsymbol{\theta}$, $\mathbf{b}^{\boldsymbol{\alpha}}_{g_1}$	$\boldsymbol{\theta}^{\boldsymbol{\alpha}}$,$\mathbf{b}^{\boldsymbol{\alpha}}_{g_1}$	$\boldsymbol{\theta}^{\boldsymbol{\beta}_1}$	$\boldsymbol{\theta}^{\boldsymbol{\alpha}}$,$\mathbf{b}^{\boldsymbol{\alpha}}_{g_1}$	0	0	0
	$\mathbf{v}_x=\mathbf{0}$ $\mathbf{v}_y=\mathbf{0}$	$\boldsymbol{\omega}=\mathbf{0}$	G	$\boldsymbol{\theta}^{\boldsymbol{\alpha}}$, $\mathbf{b}^{\boldsymbol{\alpha}}_{g_1}$	$\boldsymbol{\theta}^{\boldsymbol{\alpha}}$,$\mathbf{b}^{\boldsymbol{\alpha}}_{g_1}$	0	$\boldsymbol{\theta}^{\boldsymbol{\alpha}}$,$\mathbf{b}^{\boldsymbol{\alpha}}_{g_1}$	0	0	0
		$\boldsymbol{\omega}_x=\mathbf{0}\ \boldsymbol{\omega}_y=\mathbf{0}$	H	$\boldsymbol{\theta}^{\boldsymbol{\alpha}}$, $\mathbf{b}^{\boldsymbol{\alpha}}_{g_1}$	$\boldsymbol{\theta}^{\boldsymbol{\alpha}}$,$\mathbf{b}^{\boldsymbol{\alpha}}_{g_1}$	0	$\boldsymbol{\theta}^{\boldsymbol{\alpha}}$,$\mathbf{b}^{\boldsymbol{\alpha}}_{g_1}$	0	0	0
		Unconstrained	J	$\boldsymbol{\theta}^{\boldsymbol{\alpha}}$, $\mathbf{b}^{\boldsymbol{\alpha}}_{g_1}$	$\boldsymbol{\theta}^{\boldsymbol{\alpha}}$,$\mathbf{b}^{\boldsymbol{\alpha}}_{g_1}$	0	$\boldsymbol{\theta}^{\boldsymbol{\alpha}}$,$\mathbf{b}^{\boldsymbol{\alpha}}_{g_1}$	0	0	0
$\mathbf{p}_x\neq\mathbf{0}$ $\mathbf{p}_y\neq\mathbf{0}$ $\mathbf{p}_z\neq\mathbf{0}$	$\mathbf{v}=\mathbf{0}$	$\boldsymbol{\omega}=\mathbf{0}$	K	$\boldsymbol{\theta}$, $\mathbf{b}^{\boldsymbol{\alpha}}_{g_1}$	$\boldsymbol{\theta}^{\boldsymbol{\alpha}}$,$\mathbf{b}^{\boldsymbol{\alpha}}_{g_1}$	$\boldsymbol{\theta}^{\boldsymbol{\beta}_1}$	0	0	0	0
		$\boldsymbol{\omega}_x=\mathbf{0}\ \boldsymbol{\omega}_y=\mathbf{0}$	L	$\boldsymbol{\theta}$, $\mathbf{b}^{\boldsymbol{\alpha}}_{g_1}$	$\boldsymbol{\theta}^{\boldsymbol{\alpha}}$,$\mathbf{b}^{\boldsymbol{\alpha}}_{g_1}$	$\boldsymbol{\theta}^{\boldsymbol{\beta}_1}$	0	0	0	0
		Unconstrained	M	$\boldsymbol{\theta}$, $\mathbf{b}^{\boldsymbol{\alpha}}_{g_1}$	$\boldsymbol{\theta}^{\boldsymbol{\alpha}}$,$\mathbf{b}^{\boldsymbol{\alpha}}_{g_1}$	$\boldsymbol{\theta}^{\boldsymbol{\beta}_1}$	0	0	0	0
	$\mathbf{v}_x=\mathbf{0}$ $\mathbf{v}_y=\mathbf{0}$	$\boldsymbol{\omega}=\mathbf{0}$	N	$\boldsymbol{\theta}^{\boldsymbol{\alpha}}$, $\mathbf{b}^{\boldsymbol{\alpha}}_{g_1}$	$\boldsymbol{\theta}^{\boldsymbol{\alpha}}$,$\mathbf{b}^{\boldsymbol{\alpha}}_{g_1}$	0	0	0	0	0
		$\boldsymbol{\omega}_x=\mathbf{0}\ \boldsymbol{\omega}_y=\mathbf{0}$	O	$\boldsymbol{\theta}^{\boldsymbol{\alpha}}$, $\mathbf{b}^{\boldsymbol{\alpha}}_{g_1}$	$\boldsymbol{\theta}^{\boldsymbol{\alpha}}$,$\mathbf{b}^{\boldsymbol{\alpha}}_{g_1}$	0	0	0	0	0
		Unconstrained	P	$\boldsymbol{\theta}^{\boldsymbol{\alpha}}$, $\mathbf{b}^{\boldsymbol{\alpha}}_{g_1}$	$\boldsymbol{\theta}^{\boldsymbol{\alpha}}$,$\mathbf{b}^{\boldsymbol{\alpha}}_{g_1}$	0	0	0	0	0
	Uncon-strained	$\boldsymbol{\omega}=\mathbf{0}$	Q	0	0	0	0	0	0	0
		$\boldsymbol{\omega}_x=\mathbf{0}\ \boldsymbol{\omega}_y=\mathbf{0}$	R	0	0	0	0	0	0	0
		Unconstrained	S	0	0	0	0	0	0	0

The special motions we consider here, as well as their classifications, are the same with Table (I). $\boldsymbol{\theta}$ (composed of $\boldsymbol{\theta}^{\boldsymbol{\beta}_1}$, $\boldsymbol{\theta}^{\boldsymbol{\beta}_2}$, and $\boldsymbol{\theta}^{\boldsymbol{\alpha}}$), $\boldsymbol{\theta}^{\boldsymbol{\alpha}}$, $\boldsymbol{\theta}^{\boldsymbol{\beta}_1}$, and $\mathbf{b}^{\boldsymbol{\alpha}}_{g_1}$ denote the additional unobservable directions. In this table, $\boldsymbol{\alpha}$ follows the same definition with Table (I), and for case Col-I, $\boldsymbol{\beta}_1$ and $\boldsymbol{\beta}_2$ constitute an orthogonal basis perpendicular to $\boldsymbol{\alpha}$, while for case Col-III, $\boldsymbol{\beta}_1$ is the constant direction of ${}^{I_1}\mathbf{v}$. Note that, the total unobservable directions with only $\mathbf{dp}$ measurement are obtained by adding together Table (I) and Table (II).

†Cols I-VII represent motion constraints of the reference IMU, i.e., the local ${}^{I_1}\boldsymbol{\omega}$, ${}^{I_1}\mathbf{a}$, ${}^{I_1}\mathbf{v}$ of $\{I_1\}$. Based on the definition of $\boldsymbol{\alpha}$, examples of Cols I-VII are: stationary, uniform linear or uniform acceleration linear motion with no rotation (Col-I); linear motion along gravity direction with no rotation (Col-II); linear motion in a non-gravity direction with no rotation (Col-III); rotating around gravity in place or with uniform linear translation (Col-IV); planar motion on a horizontal surface (Col-V); planar motion on an inclined surface (Col-VI); free 3D motion (Col-VII).

‡Rows A-S represent motion constraints of the target IMU wrt the reference IMU, i.e., the relative ${}^{I_1}\mathbf{p}_{I_2}$, ${}^{I_1}\mathbf{v}_{I_2}$, ${}^{I_1}\boldsymbol{\omega}_{I_2}$ between $\{I_1\}$ and $\{I_2\}$. Without loss of generality, we align z-axis of the reference IMU at initial moment with $\boldsymbol{\alpha}$, and x, y-axis are the perpendicular directions. We use $\mathbf{p}_j=0$, $\mathbf{v}_j=0$, and $\boldsymbol{\omega}_j=0$, $j=x,y,z$, to represent that the relative position (${}^{I_1}\mathbf{p}_{I_2}$), relative linear velocity (${}^{I_1}\mathbf{v}_{I_2}$), and relative angular velocity (${}^{I_1}\boldsymbol{\omega}_{I_2}=\mathbf{C}({}^{I_1}\mathbf{q}_{I_2})\,{}^{I_2}\boldsymbol{\omega}-{}^{I_1}\boldsymbol{\omega}$) has constant zero for its j-th element, respectively, while $\neq 0$ to denote this element is non-zero for certain time steps.

$$\left[\underbrace{\overbrace{\boldsymbol{\theta}^{\boldsymbol{\beta}_1} \mid \boldsymbol{\theta}^{\boldsymbol{\beta}_2}}^{\boldsymbol{\theta}^{\boldsymbol{\beta}}{}_{21\times 2}} \mid \boldsymbol{\theta}^{\boldsymbol{\alpha}}}_{\boldsymbol{\theta}_{21\times 3}} \mid \mathbf{b}_{g_1}^{\boldsymbol{\alpha}}\right]_{[21\times 1,\ 21\times 1,\ 21\times 1,\ 21\times 1]} \tag{17}$$

$$= \begin{bmatrix} \mathbf{0}_{3\times 2} & \mathbf{0}_{3\times 1} & \mathbf{0}_{3\times 1} \\ \mathbf{0}_{3\times 2} & \mathbf{0}_{3\times 1} & \mathbf{0}_{3\times 1} \\ \mathbf{C}^T({}^{I_1}\mathbf{q}_{I_2}(t_0))\,[\boldsymbol{\beta}_1 \quad \boldsymbol{\beta}_2] & \mathbf{C}^T({}^{I_1}\mathbf{q}_{I_2}(t_0))\boldsymbol{\alpha} & \mathbf{0}_{3\times 1} \\ \mathbf{0}_{3\times 2} & \mathbf{0}_{3\times 1} & \boldsymbol{\alpha} \\ \mathbf{0}_{3\times 2} & \mathbf{0}_{3\times 1} & \mathbf{0}_{3\times 1} \\ [\boldsymbol{\alpha}\times\boldsymbol{\beta}_1 \quad \boldsymbol{\alpha}\times\boldsymbol{\beta}_2] & \mathbf{0}_{3\times 1} & \mathbf{0}_{3\times 1} \\ \mathbf{0}_{3\times 2} & \mathbf{0}_{3\times 1} & \mathbf{0}_{3\times 1} \end{bmatrix}$$

where $\boldsymbol{\alpha}$, $\boldsymbol{\beta}_1$, $\boldsymbol{\beta}_2$ are defined in Table (II). And the physical meaning of each direction is:

- $\mathbf{b}_{g_1}^{\boldsymbol{\alpha}}$ is 1 dof of the absolute gyroscope bias of reference IMU along $\boldsymbol{\alpha}$ direction.
- $\boldsymbol{\theta}^{\boldsymbol{\alpha}}$ is 1 dof of the relative orientation about the $\boldsymbol{\alpha}$ direction, i.e., the yaw angle with respect to $\boldsymbol{\alpha}$.
- $\boldsymbol{\theta}^{\boldsymbol{\beta}}$ is 2 dof of the relative orientation about the $\boldsymbol{\beta}$ directions, i.e., the two tilt angles with respect to $\boldsymbol{\alpha}$, and coupled with the absolute accelerometer bias of reference IMU along $\boldsymbol{\beta}$ directions.
- $\boldsymbol{\theta}^{\boldsymbol{\beta}_1}$ is 1 dof of the relative orientation about the $\boldsymbol{\beta}_1$ direction, and coupled with the absolute accelerometer bias of reference IMU along $\boldsymbol{\alpha}\times\boldsymbol{\beta}_1$ direction.

In summary, we have shown that these special motions can introduce multiple unobservable directions to the system. We can classify all these cases into two categories: The first category is when certain components of the relative orientation are unobservable (all non-zero cells in Table (II)), e.g., when a vehicle stays still or in uniform linear motion, while an HMD purely rotates inside the vehicle. The second category is when only biases may be unobservable (all other cells in Table (I)), e.g., when either agent undergoes sufficient motion, while the other agent can be moving or stationary. In practice, a mobile agent's motion is typically the combination of general and special motions, with each mode occupying certain periods of time. As shown in [28], "approximate" or intermittent special motion profiles may cause estimation inaccuracy issues as well. Therefore, according to our observability analysis, if the two agents follow special motions in the first category, even if it is only approximate, the system with only $\mathbf{dp}$ measurement may have a large estimation error along the unobservable directions of the relative orientation (e.g., relative yaw error). Otherwise, if the agents follow special motions in the second category, then individual IMU bias estimates may be unreliable, but the relative pose states, since they are observable, can be accurate.

VI. Numerical Simulation

In order to verify the unobservable directions under special motions in the preceding section and show their impact on the state estimates, we conduct Monte Carlo simulations based on EKF. For each motion case, we execute 50 independent runs with random noise inputs, and calculate the root mean square error (RMSE) [37] and 3σ bound for each state per time step, serving as an assessment of the accuracy and consistency of the estimates. We choose four typical motion patterns corresponding to Cell I-K, III-K, V-K, and I-S of Table (I) and Table (II).

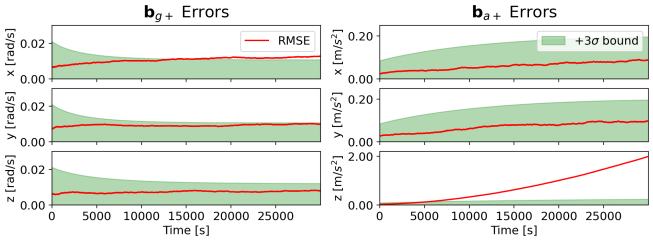

Fig. 2. The RMSE and 3σ bound of composite biases for motion I-K of Table (I), i.e., both IMUs stay still, with both $\mathbf{dp}$ and $\mathbf{dq}$ measurements.

For Cell I-K in Table (I), even with both $\mathbf{dp}$ and $\mathbf{dq}$ measurements, when both IMUs remain still, all 6 directions of $\mathbf{b}_{g+}$ and $\mathbf{b}_{a+}$ (see (16)) are unobservable. From Fig. 2, we can see that none of the errors in 3 directions of $\mathbf{b}_{g+}$ converges. The error along the z direction of $\mathbf{b}_{a+}$ rapidly grows and exceeds the 3σ bound, while the errors and 3σ bounds of the other 2 directions continuously increase.

When there is only $\mathbf{dp}$ measurement, in addition to biases, unobservable directions can also arise for relative orientation. For Cell I-K in Table (II), the 3 directions of orientation are all unobservable, and from Fig. 3(a), the yaw error rapidly grows and significantly exceeds the 3σ bound, while the errors of the other 2 angles and their 3σ bounds continuously increase. For Cell III-K, only the roll (the orientation around the x direction) is unobservable, and from Fig. 3(b) the error and 3σ bound of just the roll angle keep increasing. For Cell V-K and I-S, all 3 directions of orientation are observable, and from Fig. 3(c) and (d) all errors rapidly decrease to very small values and remain well within the 3σ bounds. Overall, from Fig. 3(a) to (c), as the motion of the reference IMU becomes increasingly sufficient, unobservable directions of orientation disappear. And from Fig. 3(c) and (d), it is evident that as long as the motion of either IMU is sufficient, the estimates of relative orientation are reliable.

For more comprehensive simulation results see Sect. VI in our Supp. Mater. [33]. All simulation results validate our observability findings in Sect. V perfectly.

VII. Experimental Results

In this section, we design experiments to showcase the performance of the Dual-IMU state estimation system in real-world applications. In our experiment, both the reference and target IMUs are consumer-grade MEMS-IMUs, where the reference IMU is attached to a moving vehicle and the target IMU comes from an HMD. Images from the HMD's camera of a car-fixed ArUco marker are processed by OpenCV's built-in algorithms [38] to calculate relative poses, serving as $\mathbf{dp}$ and $\mathbf{dq}$ measurements. The ground truth is provided by an OptiTrack [39] system attached to the vehicle. In the experimental route (about 30mins), the vehicle's motion is highly diverse, as shown in the bottom subplot of Fig. 4. We drive the vehicle along this route twice, and a person sitting inside the vehicle and wearing the HMD exhibits two different motion patterns: attempting to remain still and moving normally. For each motion case, we test three setups depending on whether the initial biases are calibrated and

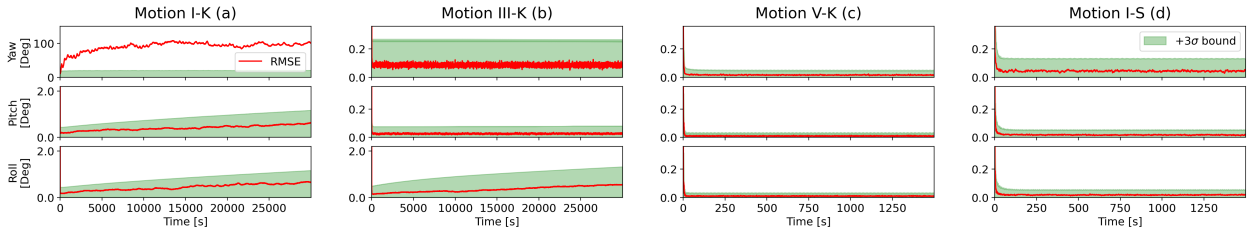

Fig. 3. The RMSE and 3σ bound of relative orientation estimates for different motion patterns with only $\mathbf{dp}$ measurement. (a), (b), (c), and (d) correspond to the motion patterns described in Cell I-K, III-K, V-K, and I-S of Table (II), respectively. Specifically, for Cell I-K, III-K, and V-K, the reference IMU remains still, moves along a straight line (the x direction), and moves on a horizontal plane, respectively. Meanwhile, in these three cases, the target IMU remains still with respect to the reference IMU. Lastly, for Cell I-S, the reference IMU remains still, while the target IMU moves genericly.

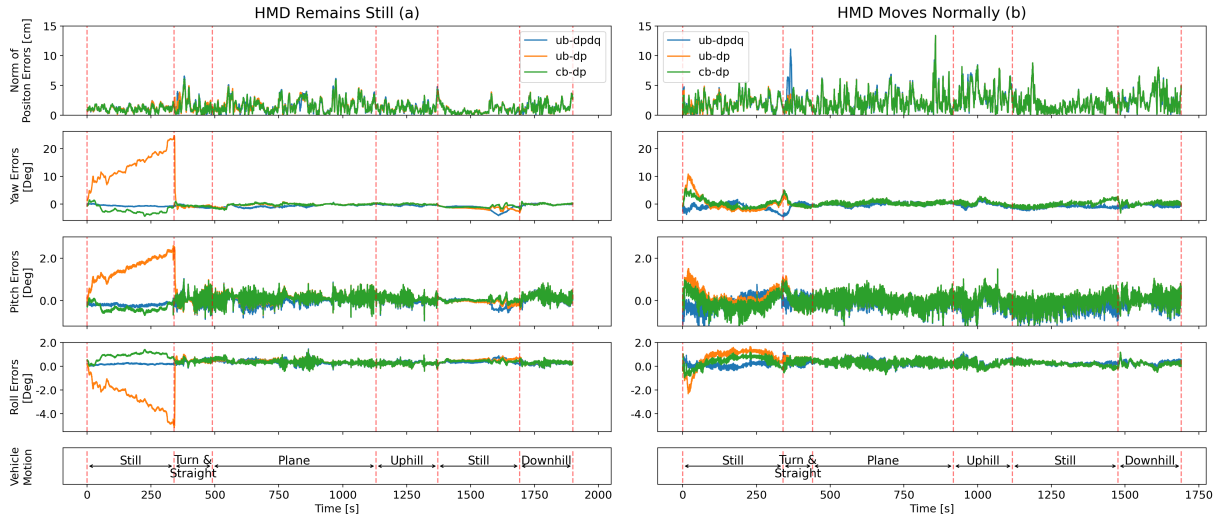

Fig. 4. Comparison of relative pose errors under different motions of the HMD and the vehicle, as well as under different estimation setups. Specifically, for the initial biases, we consider uncalibrated biases (ub) and calibrated biases (cb). As for the measurements used, we evaluate the system with both $\mathbf{dp}$ and $\mathbf{dq}$ (dpdq) and with $\mathbf{dp}$ only (dp). Note that, the results of cb-dpdq are almost identical with ub-dpdq, and are omitted.

whether there is $\mathbf{dq}$ measurement (see Fig. 4). Our estimation implementation is based on EKF, where each prediction and update cycle takes $20\mu s$ (ArUco marker processing time excluded) on an Intel (i7, 2.3GHz) processor.

As shown in Fig. 4, the errors of relative pose estimates with both $\mathbf{dp}$ and $\mathbf{dq}$ measurements are consistently small, because the relative pose is directly measured and hence observable from Table (I). Meanwhile, with only $\mathbf{dp}$ measurement, the pose errors are largely affected by the motion periods. From Fig. 4(a), in the initial phase, both the vehicle and HMD remain still, and from Cell I-K in Table (II), the relative orientation are unobservable. Hence, we can see that with uncalibrated biases, the angle errors, especially the yaw ($\boldsymbol{\theta}^{\boldsymbol{\alpha}}$) error, continue to increase to a big amount, while with calibrated biases, the errors still exist but are smaller. This also indicates that at this stage, biases (e.g., $\mathbf{b}_{g_1}^{\boldsymbol{\alpha}}$) are not observable. Next, the vehicle starts moving (turn and straight), which corresponds to planar motion in Cell V-K of Table (II) and hence the relative orientation becomes observable, then the angle errors quickly converge. Later on, when both IMUs come to the second stationary period, since gyroscope biases have already converged due to previous motions corresponding to Cell VII-K in Table (I) and (II), the accuracy remains high. Moreover, when comparing Fig. 4(b) with (a), we can see that with uncalibrated biases, the HMD moving normally (Row-S in Table (II)) results in better relative orientation estimates than staying still (Row-K in Table (II)). Note that, the position errors of Fig. 4(b) are slightly larger than (a), because the tracking quality of the ArUco marker degrades as the HMD's camera moves faster.

To summarize, the experimental results align well with our observability analysis in Sect. V. Overall, the proposed algorithm achieves satisfactory relative localization on real-world data and runs extremely fast ($20\mu s$ per process). To further improve localization accuracy, one can enlarge the marker's size, design special markers, use outside-in tracking systems, or introduce additional observations to the vehicle.

VIII. Conclusions

In this paper, we presented a Dual-IMU state estimation system, which jointly estimates the relative pose, velocity, and all four biases from the two IMUs. For this system, we proved that it is locally weakly observable when both IMUs undergo general motion, even with only relative position observation. Furthermore, we have identified the system's unobservable directions across various special motions and categorized these motions into two groups: those resulting in the relative orientation becoming unobservable, and those potentially leading to only biases being unobservable. Through numerical simulations and real-world experiments, our observability findings were validated based on the estimation error and consistency, where the relative orientation estimates were degraded or unaffected, depending on the corresponding motion category. Lastly, in the real world, our system was able to localize an HMD with respect to a moving vehicle with high accuracy and computational efficiency.

REFERENCES

[1] D. Fox, W. Burgard, H. Kruppa, and S. Thrun, "Collaborative multi-robot localization," in *Proc. of the 23rd German Conference on Artificial Intelligence*. Springer, 1999, pp. 15–26.

[2] L. Freda and G. Oriolo, "Vision-based interception of a moving target with a nonholonomic mobile robot," *Robotics and Autonomous Systems*, vol. 55, no. 6, pp. 419–432, June 2007.

[3] D. B. Wilson, A. H. Göktoğan, and S. Sukkarieh, "A vision based relative navigation framework for formation flight," in *Proc. of the IEEE International Conference on Robotics and Automation (ICRA)*, 2014, pp. 4988–4995.

[4] J. Haeling, C. Winkler, S. Leenders, D. Keßelheim, A. Hildebrand, and M. Necker, "In-car 6-dof mixed reality for rear-seat and co-driver entertainment," in *Proc. of the IEEE Conference on Virtual Reality and 3D User Interfaces (VR)*, 2018, pp. 757–758.

[5] D. Titterton and J. L. Weston, *Strapdown inertial navigation technology*. Institution of Engineering and Technology, 2004.

[6] M. S. Grewal, L. R. Weill, and A. P. Andrews, *Global positioning systems, inertial navigation, and integration*. John Wiley & Sons, 2007, ch. 10.

[7] X. S. Zhou and S. I. Roumeliotis, "Determining 3-d relative transformations for any combination of range and bearing measurements," *IEEE Transactions on Robotics*, vol. 29, no. 2, pp. 458–474, April 2013.

[8] R. Hermann and A. Krener, "Nonlinear controllability and observability," *IEEE Transactions on Automatic Control*, vol. 22, no. 5, pp. 728–740, October 1977.

[9] G. P. Huang, A. I. Mourikis, and S. I. Roumeliotis, "Observability-based rules for designing consistent ekf slam estimators," *The International Journal of Robotics Research*, vol. 29, no. 5, pp. 502–528, April 2010.

[10] E.-H. Shin and N. El-Sheimy, "Accuracy improvement of low cost ins/gps for land applications," in *Proc. of the National Technical Meeting of The Institute of Navigation*, 2002, pp. 146–157.

[11] W. Wen, X. Bai, Y. C. Kan, and L.-T. Hsu, "Tightly coupled gnss/ins integration via factor graph and aided by fish-eye camera," *IEEE Transactions on Vehicular Technology*, vol. 68, no. 11, pp. 10 651–10 662, November 2019.

[12] G. P. Huang, "Visual-inertial navigation: A concise review," in *Proc. of the IEEE International Conference on Robotics and Automation (ICRA)*, 2019, pp. 9572–9582.

[13] A. I. Mourikis and S. I. Roumeliotis, "A multi-state constraint kalman filter for vision-aided inertial navigation," in *Proc. of the IEEE International Conference on Robotics and Automation (ICRA)*, 2007, pp. 3565–3572.

[14] T. Qin, P. Li, and S. Shen, "Vins-mono: A robust and versatile monocular visual-inertial state estimator," *IEEE Transactions on Robotics*, vol. 34, no. 4, pp. 1004–1020, August 2018.

[15] C. Campos, R. Elvira, J. J. G. Rodríguez, J. M. Montiel, and J. D. Tardós, "Orb-slam3: An accurate open-source library for visual, visual–inertial, and multimap slam," *IEEE Transactions on Robotics*, vol. 37, no. 6, pp. 1874–1890, December 2021.

[16] T. Shan, B. Englot, D. Meyers, W. Wang, C. Ratti, and D. Rus, "Lio-sam: Tightly-coupled lidar inertial odometry via smoothing and mapping," in *Proc. of the IEEE/RSJ International Conference on Intelligent Robots and Systems (IROS)*, 2020, pp. 5135–5142.

[17] W. Xu, Y. Cai, D. He, J. Lin, and F. Zhang, "Fast-lio2: Fast direct lidar-inertial odometry," *IEEE Transactions on Robotics*, vol. 38, no. 4, pp. 2053–2073, August 2022.

[18] S. I. Roumeliotis and G. A. Bekey, "Distributed multirobot localization," *IEEE Transactions on Robotics and Automation*, vol. 18, no. 5, pp. 781–795, October 2002.

[19] A. Martinelli, A. Oliva, and B. Mourrain, "Cooperative visual-inertial sensor fusion: The analytic solution," *IEEE Robotics and Automation Letters*, vol. 4, no. 2, pp. 453–460, April 2019.

[20] B. Kim, M. Kaess, L. Fletcher, J. Leonard, A. Bachrach, N. Roy, and S. Teller, "Multiple relative pose graphs for robust cooperative mapping," in *Proc. of the IEEE International Conference on Robotics and Automation (ICRA)*, 2010, pp. 3185–3192.

[21] S. Choudhary, L. Carlone, C. Nieto, J. Rogers, H. I. Christensen, and F. Dellaert, "Distributed mapping with privacy and communication constraints: Lightweight algorithms and object-based models," *The International Journal of Robotics Research*, vol. 36, no. 12, pp. 1286–1311, October 2017.

[22] C.-S. Jao, Y. Wang, and A. M. Shkel, "Pedestrian inertial navigation system augmented by vision-based foot-to-foot relative position measurements," in *Proc. of the IEEE/ION Position, Location and Navigation Symposium (PLANS)*, 2020, pp. 900–907.

[23] A. M. Fosbury and J. L. Crassidis, "Relative navigation of air vehicles," *Journal of Guidance, Control, and Dynamics*, vol. 31, no. 4, pp. 824–834, July 2008.

[24] F. Aghili and C.-Y. Su, "Robust relative navigation by integration of icp and adaptive kalman filter using laser scanner and imu," *IEEE/ASME Transactions on Mechatronics*, vol. 21, no. 4, pp. 2015–2026, August 2016.

[25] A. Martinelli, "Vision and imu data fusion: Closed-form solutions for attitude, speed, absolute scale, and bias determination," *IEEE Transactions on Robotics*, vol. 28, no. 1, pp. 44–60, February 2012.

[26] J. A. Hesch, D. G. Kottas, S. L. Bowman, and S. I. Roumeliotis, "Consistency analysis and improvement of vision-aided inertial navigation," *IEEE Transactions on Robotics*, vol. 30, no. 1, pp. 158–176, February 2013.

[27] A. Martinelli, "Vision and imu data fusion: Closed-form solutions for attitude, speed, absolute scale, and bias determination," *IEEE Transactions on Robotics*, vol. 28, no. 1, pp. 44–60, February 2011.

[28] K. J. Wu, C. X. Guo, G. Georgiou, and S. I. Roumeliotis, "Vins on wheels," in *Proc. of the IEEE International Conference on Robotics and Automation (ICRA)*, 2017, pp. 5155–5162.

[29] G. P. Huang, A. I. Mourikis, and S. I. Roumeliotis, "A first-estimates jacobian ekf for improving slam consistency," in *Proc. of the Experimental Robotics: The Eleventh International Symposium*. Springer, 2009, pp. 373–382.

[30] C. Chen, P. Geneva, Y. Peng, W. Lee, and G. P. Huang, "Optimization-based vins: Consistency, marginalization, and fej," in *Proc. of the IEEE/RSJ International Conference on Intelligent Robots and Systems (IROS)*, 2023, pp. 1517–1524.

[31] G. P. Huang, N. Trawny, A. I. Mourikis, and S. I. Roumeliotis, "Observability-based consistent ekf estimators for multi-robot cooperative localization," *Autonomous Robots*, vol. 30, pp. 99–122, January 2011.

[32] A. Cristofaro and A. Martinelli, "3d cooperative localization and mapping: Observability analysis," in *Proc. of the IEEE American Control Conference*, 2011, pp. 1630–1635.

[33] (Supplementary Material), W. Lai, R. Guo, and K. J. Wu, "Dual-imu state estimation for relative localization of two mobile agents," *arXiv preprint arXiv:2402.18394*, 2024. [Online]. Available: https://arxiv.org/abs/2402.18394

[34] J. Sola, "Quaternion kinematics for the error-state kalman filter," *arXiv preprint arXiv:1711.02508*, 2017.

[35] R. Kümmerle, G. Grisetti, H. Strasdat, K. Konolige, and W. Burgard, "g2o: A general framework for graph optimization," in *Proc. of the IEEE International Conference on Robotics and Automation (ICRA)*, 2011, pp. 3607–3613.

[36] Z. Chen, K. Jiang, and J. C. Hung, "Local observability matrix and its application to observability analyses," in *Proc. of the IECON'90: 16th Annual Conference of IEEE Industrial Electronics Society*, 1990, pp. 100–103.

[37] Y. Bar-Shalom, X. R. Li, and T. Kirubarajan, *Estimation with applications to tracking and navigation: theory algorithms and software*. John Wiley & Sons, 2001.

[38] "Opencv modules: Detection of aruco markers," https://docs.opencv.org/4.x/d5/dae/tutorial_aruco_detection.html.

[39] "Optitrack," https://optitrack.com/.